Rapid Surface-Wave Dispersion and Plane-Wave Reflection Analyses of Planar Corrugated Surfaces by Asymptotic Corrugations Boundary Conditions Even for Oblique Azimuth Planes

Malcolm Ng Mou Kehn, *Member, IEEE*

***Abstract*—The asymptotic corrugations boundary condition (ACBC) is used together with classical theory of vector potentials to analyze planar corrugations. A transcendental characteristic equation is derived, from which the dispersion diagram can be obtained, thereby conveying surface wave passband and stopband properties, even for propagation within oblique azimuth planes as well as both principal TE and TM polarizations. From the formulation, field distributions for the regions within the grooves and above the corrugations can also be generated. When compared with the dispersion graphs obtained from characteristic equations derived by the classical transverse resonance technique (TRT), the newly presented ACBC method provides superior accuracy. Explicit formulas for the complex reflection coefficient (amplitude and phase) for both TE and TM polarized plane-wave incidences are also derived as closed-form analytic functions of all parameters (especially the azimuth phi angle of incidence) using a novel concept of unusual transversely phased plane-waves. These proposed approaches are massively more efficient than full-wave solvers, providing unparalleled speedup of computation by thousands of times. The surface-wave and reflection properties of planar corrugations are thus herein analyzed in a unified, complete, and elegant manner that is also highly efficient but yet accurate. This thorough work is thus a great boost to the continued use of corrugated surfaces as artificial magnetic conductors (AMC), electromagnetic bandgap (EBG) structures, and soft/hard surfaces in all walks of antenna design, especially in terms of speed and accuracy.**

***Index Terms*—Asymptotic corrugations boundary condition (ACBC), corrugations, dispersion diagram, electromagnetic bandgap (EBG) surfaces.**

I. Introduction

PLANAR corrugated surfaces have been a subject of keen interest amongst purists in electromagnetic theory for many decades [1]–[7]. With the advent of the digital computer, traditional analysis work was extended to include numerical treatments of plane-wave scattering from corrugations [8]–[10]. Theoreticians and computational enthusiasts were not the only ones captivated by this structure. Experimentalists and practical engineers have, likewise for the past many years, been making use of corrugations to develop improved microwave devices such as waveguides and antennas. Possibly the most distinct and important utility of corrugated surfaces is in realizing soft and hard surfaces [11], which provide bountiful applications [12], [13].

By providing an approximate relationship between the electric and magnetic field on a chosen surface, approximate boundary conditions (ABC) have proven effective for simplifying both analytical and numerical solutions of electromagnetic wave problems [14], [15]. Among the simplest kind is the standard impedance boundary condition (IBC), whose accuracy was improved by the extension to generalized impedance boundary conditions (GIBC). The works of [16]–[18] used such approximate impedance boundary conditions to study corrugated surfaces. In a related way, the asymptotic strip and corrugations boundary conditions (ASBC and ACBC) were introduced in [19] to treat strip-gratings and corrugations rapidly, which provide exact solutions as the periods tend to zero.

Despite these cited works, none has studied corrugated surfaces in terms of the dispersion diagram conveying the surface-wave properties especially for oblique azimuth propagation directions, or presented accurate characteristic equations from which such a diagram is obtained. Field distributions of the surface wave modes supported by the corrugations are also nowhere to be found. To the author's knowledge, neither are there publications on investigations into the reflection properties of planar corrugations, not even for the principal azimuth planes of incidences, let alone oblique ones. To conduct such studies would prove essential for a more thorough characterization of high-impedance surfaces (HIS) and artificial magnetic conductors (AMC) composed of such corrugated surfaces as opposed to just reflection studies of only the two principal azimuth planes.

In this work, planar corrugations of infinite extent shall be analyzed using the ACBC in conjunction with classical vector potential analysis, leading to the derivation of a transcendental characteristic equation, from which the surface-wave band diagrams can be generated for the principal direction (perpendicular to the grooves/ridges) as well as oblique azimuth angles of propagation. Surface-wave modal field distributions of the corrugated surface obtainable by the formulation shall

Manuscript received July 31, 2012; revised November 21, 2012; accepted December 26, 2012. Date of publication January 03, 2013; date of current version May 01, 2013. This work was supported by the National Science Council of Taiwan.

The author is with the National Chiao Tung University, Hsinchu 30010, Taiwan (e-mail: malcolm.ng@ieee.org).

Color versions of one or more of the figures in this paper are available online at http://ieeexplore.ieee.org.

Digital Object Identifier 10.1109/TAP.2013.2237742

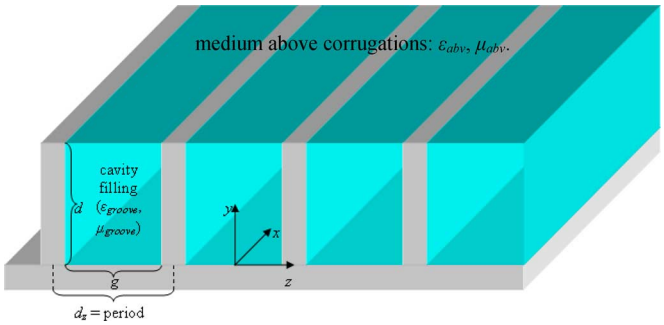

Fig. 1. Infinitely long corrugations of infinite expanse.

also be presented. The transverse resonance technique (TRT) is an alternative for deriving the characteristic equations for TM modes of the planar corrugated structure for the principal (perpendicular to the ridges) and oblique directions of surface-wave propagation, solving of which also generates the dispersion diagram. It will however be demonstrated that the accuracy of this TRT for oblique azimuth directions of surface-wave propagation is poor. We shall herein show that our new method based on ACBC overcomes this inadequacy and provides extremely accurate dispersion diagrams. In addition, by using a novel concept of considering *unusual transversely phased plane-waves*, closed-form analytic expressions for the complex reflection coefficient of both TM and TE polarized plane-wave incidence shall be derived as functions of all parameters, especially the azimuth (incidence angle as well. Numerical results computed for both the dispersion and reflection-phase diagrams will be presented, all of which are validated by two full-wave solvers: 1) commercial software CST Microwave Studio, and 2) a self-developed moment-method code [20]. It will also be shown that this ACBC method is innumerably faster in computation speed than these full-wave solvers, by thousands of times.

II. Theory and Formulation

Consider the planar corrugated surface of Fig. 1, which is parallel to the xz plane with periodicity along z and perpendicular direction along y. The period and depth of the corrugations are d_z and d, respectively. The width of each groove along z is g. The permittivity and permeability of the material filling the groove are $\varepsilon_{\text{groove}}$ and μ_{groove}, whereas ε_{abv} and μ_{abv} represent the parameters of the upper half-space above the corrugations. In the following field expressions, a universal $\exp(-jk_{x0}x)$ term has been included to represent the component of surface wave propagation along the x direction, where k_{x0} is the phase constant along x, parallel to the grooves and ridges. This term applies also to the fields within the grooves of the corrugations for phase continuity with the upper half-space region.

A. Groove Fields of Corrugations

The fields within the corrugation grooves are derived by classical vector potential analyses for TE^y and TM^y modes and the enforcement of appropriate boundary conditions requiring the vanishing of tangential electric field components on the metallic walls of the grooves [21]. Doing so, the x, y and z components of the E and H fields of the TE^y and TM^y modal fields within the groove are stated as follows:

$$\begin{bmatrix} E^{\text{groove}}_{x_{TE^y}(p)} \\ H^{\text{groove}}_{x_{TM^y}(p)} \end{bmatrix} = -\begin{bmatrix} \dfrac{A^{\text{groove}}_{TE} S_{y_{TE}} S^p_z}{\varepsilon_{\text{groove}}} \\ \dfrac{A^{\text{groove}}_{TM} C_{y_{TM}} C^p_z}{\mu_{\text{groove}}} \end{bmatrix} \frac{p\pi}{g} e^{-jk_{x0}x} \tag{1}$$

$$E^{\text{groove}}_{y_{TE^y}} = 0 \text{ and } H^{\text{groove}}_{y_{TM^y}} = 0 \tag{2}$$

$$\begin{bmatrix} E^{\text{groove}}_{z_{TE^y}(p)} \\ H^{\text{groove}}_{z_{TM^y}(p)} \end{bmatrix} = \begin{bmatrix} \dfrac{A^{\text{groove}}_{TE} S_{y_{TE}} C^p_z}{\varepsilon_{\text{groove}}} \\ \dfrac{-A^{\text{groove}}_{TM} C_{y_{TM}} S^p_z}{\mu_{\text{groove}}} \end{bmatrix} jk_{x0} e^{-jk_{x0}x} \tag{3}$$

$$\begin{bmatrix} H^{groove}_{x_{TE^y}(p)} \\ E^{\text{groove}}_{x_{TM^y}(p)} \end{bmatrix} = \begin{bmatrix} -A^{\text{groove}}_{TE} k^{\text{groove}}_{y_{TE}} C_{y_{TE}} C^p_z \\ A^{\text{groove}}_{TM} k^{\text{groove}}_{y_{TM}} S_{y_{TM}} S^p_z \end{bmatrix} \times \frac{k_{x0} e^{-jk_{x0}x}}{\omega \mu_{\text{groove}} \varepsilon_{\text{groove}}} \tag{4}$$

$$\begin{Bmatrix} H^{\text{groove}}_{y_{TE^y}(p)} \\ E^{\text{groove}}_{y_{TM^y}(p)} \end{Bmatrix} = \begin{Bmatrix} A^{\text{groove}}_{TE} \left[k^2_{\text{groove}} - \left(k^{\text{groove}}_{y_{TE}}\right)^2\right] S_{y_{TE}} C^p_z \\ A^{\text{groove}}_{TM} \left[k^2_{\text{groove}} - \left(k^{\text{groove}}_{y_{TM}}\right)^2\right] C_{y_{TM}} S^p_z \end{Bmatrix} \times \frac{e^{-jk_{x0}x}}{j\omega \mu_{\text{groove}} \varepsilon_{\text{groove}}} \tag{5}$$

$$\begin{bmatrix} H^{\text{groove}}_{z_{TE^y}(p)} \\ E^{\text{groove}}_{z_{TM^y}(p)} \end{bmatrix} = -\begin{bmatrix} A^{\text{groove}}_{TE} k^{\text{groove}}_{y_{TE}} C_{y_{TE}} S^p_z \\ A^{\text{groove}}_{TM} k^{\text{groove}}_{y_{TM}} S_{y_{TM}} C^p_z \end{bmatrix} \times \frac{\left(\frac{p\pi}{g}\right) e^{-jk_{x0}x}}{j\omega \mu_{\text{groove}} \varepsilon_{\text{groove}}} \tag{6}$$

where

$$\begin{bmatrix} C_{y_{T\zeta}} \\ S_{y_{T\zeta}} \end{bmatrix} = \begin{bmatrix} \cos\left(k^{\text{groove}}_{y_{T\zeta}} y\right) \\ \sin\left(k^{\text{groove}}_{y_{T\zeta}} y\right) \end{bmatrix} \text{ and } \begin{Bmatrix} C^p_z \\ S^p_z \end{Bmatrix} = \begin{Bmatrix} \cos\left[\frac{p\pi}{g}\left(z + \frac{g}{2}\right)\right] \\ \sin\left[\frac{p\pi}{g}\left(z + \frac{g}{2}\right)\right] \end{Bmatrix}$$

in which ζ may be E or M. The wavenumber of the medium filling the groove is $k_{\text{groove}} = \omega\sqrt{(\mu_{\text{groove}}\varepsilon_{\text{groove}})}$, with $\omega = 2\pi f$ being the angular frequency [rad/s]. $A^{\text{groove}}_{T\zeta}$ represents the amplitude coefficient of the $\text{T}\zeta$ mode within the groove, and p is an integer symbolizing the modal index representing the number of half-cycle variations along z. With phase continuity being the reason, k_{x0} is the universal wavenumber along x shared by both the presently considered groove region as well as the upper-half space above the corrugations (the latter as elaborated in the next subsection). $k^{\text{groove}}_{y_{T\zeta}}$ is the wavenumber along y in the groove for the $\text{T}\zeta$ mode. Obviously, all subscripts or superscripts "*groove*" signify that their associated quantities pertain to the groove region. The symbols C and S are introduced to abbreviate the notation.

B. Modal Fields Within Upper Half-Space Above Corrugations ($y > d$)

Likewise, by vector potential analysis as well, the various components of the E and H fields of the TE^y and TM^y modal

fields in the upper half-space region above the corrugations are stated as follows:

$$\begin{bmatrix} E^{\text{above}}_{x_{TE}y} \\ E^{\text{above}}_{z_{TE}y} \end{bmatrix} = A^{\text{above}}_{TE} \begin{bmatrix} -k^{\text{above}}_{z_{TE}} \\ k_{x0} \end{bmatrix} \times \frac{je^{-jk_{x0}x}e^{-jk^{\text{above}}_{y_{TE}}(y-d)}e^{-jk^{\text{above}}_{z_{TE}}z}}{\varepsilon_{abv}} \tag{7}$$

$$E^{\text{above}}_{y_{TE}y} = 0 \text{ and } H^{\text{above}}_{y_{TM}y} = 0 \tag{8}$$

$$\begin{bmatrix} H^{\text{above}}_{x_{TE}y} \\ H^{\text{above}}_{y_{TE}y} \\ H^{\text{above}}_{z_{TE}y} \end{bmatrix} = A^{\text{above}}_{TE} \begin{bmatrix} -k_{x0}k^{\text{above}}_{y_{TE}} \\ k^2_{\text{above}} - \left(k^{\text{above}}_{y_{TE}}\right)^2 \\ -k^{\text{above}}_{y_{TE}}k^{\text{above}}_{z_{TE}} \end{bmatrix} \times \frac{e^{-jk_{x0}x}e^{-jk^{\text{above}}_{y_{TE}}(y-d)}e^{-jk^{\text{above}}_{z_{TE}}z}}{j\omega\mu_{abv}\varepsilon_{abv}} \tag{9}$$

$$\begin{bmatrix} E^{\text{above}}_{x_{TM}y} \\ E^{\text{above}}_{y_{TM}y} \\ E^{\text{above}}_{z_{TM}y} \end{bmatrix} = A^{\text{above}}_{TM} \begin{bmatrix} -k_{x0}k^{\text{above}}_{y_{TM}} \\ k^2_{\text{above}} - \left(k^{\text{above}}_{y_{TM}}\right)^2 \\ -k^{\text{above}}_{y_{TM}}k^{\text{above}}_{z_{TM}} \end{bmatrix} \times \frac{e^{-jk_{x0}x}e^{-jk^{\text{above}}_{y_{TM}}(y-d)}e^{-jk^{\text{above}}_{z_{TM}}z}}{j\omega\mu_{abv}\varepsilon_{abv}} \tag{10}$$

$$\begin{bmatrix} H^{above}_{x_{TM}y} \\ H^{\text{above}}_{z_{TM}y} \end{bmatrix} = A^{\text{above}}_{TM} \begin{bmatrix} k^{\text{above}}_{z_{TM}} \\ -k_{x0} \end{bmatrix} \times \frac{je^{-jk_{x0}x}e^{-jk^{\text{above}}_{y_{TM}}(y-d)}e^{-jk^{\text{above}}_{z_{TM}}z}}{\mu_{abv}} \tag{11}$$

where A^{above}_{TE} and A^{above}_{TM} represent the amplitude coefficients of the TE and TM modes, respectively, in the upper half-space above the corrugated surface. Similar to the groove region, $k^{\text{above}}_{y_{TE}}$ and $k^{\text{above}}_{y_{TM}}$ are the wavenumbers along y in the upper half-space region for the TE and TM modes, respectively. Likewise, $k^{\text{above}}_{z_{TE}}$ and $k^{\text{above}}_{z_{TM}}$ are the corresponding wavenumbers along z. As obvious as before, all subscripts or superscripts "*above*" indicate that their associated quantities pertain to the upper half-space region above the corrugations.

C. Asymptotic Corrugations Boundary Conditions (ACBC)

Defining first the unit vector parallel and orthogonal to the corrugations as $\hat{a}_p$ and $\hat{a}_o$, respectively, which for our configuration of Fig. 1 are $\hat{x}$ and $\hat{z}$, the asymptotic corrugations boundary conditions (ACBC) are stated as follows:

$$\vec{E}^{\text{groove}} \cdot \hat{a}_p = 0 \tag{12}$$

$$\vec{E}^{\text{above}} \cdot \hat{a}_p = 0 \tag{13}$$

$$\vec{E}^{\text{groove}} \cdot \hat{a}_o = \vec{E}^{\text{above}} \cdot \hat{a}_o \tag{14}$$

$$\vec{H}^{\text{groove}} \cdot \hat{a}_p = \vec{H}^{\text{above}} \cdot \hat{a}_p \tag{15}$$

where

$$\vec{E}^{\text{groove}} = \sum_{p_{TE}} \left[\hat{x}E^{\text{groove}}_{x_{TE}y\,(p_{TE})} + \hat{z}E^{\text{groove}}_{z_{TE}y\,(p_{TE})}\right] + \sum_{p_{TM}} \left[\hat{x}E^{\text{groove}}_{x_{TM}y\,(p_{TM})} + \hat{y}E^{\text{groove}}_{y_{TM}y\,(p_{TM})} + \hat{z}E^{\text{groove}}_{z_{TM}y\,(p_{TM})}\right]$$

noting the incorporated subscripts TE and TM to the integer modal index p to distinguish between the mode types. Now, coming to a crucial step, assume $p_{TE} = 0$ and $p_{TM} = 0$ in the grooves, i.e., existence of only the dominant $p_{TE} = 0$ (TEM) mode and absence of all TM modes, thereby having just simply $\vec{E}^{\text{groove}}_{p_{TE}=0} = \hat{z}E^{\text{groove}}_{z_{TE}y\,(p_{TE}=0)}$ in place of $\vec{E}^{\text{groove}}$ in (12) and (14). For (12), it is observed, respectively from the upper equation of (1) and the lower equation of (4) that

$$E^{\text{groove}}_{x_{TE}y}(y=d) = 0 \quad \text{and} \quad E^{\text{groove}}_{x_{TM}y}(y=d) = 0 \tag{16}$$

are already satisfied by the $p_{TE} = 0$ and $p_{TM} = 0$ conditions under ACBC. As for (13), we require

$$E^{\text{above}}_{x_{TE}y}(y=d) + E^{\text{above}}_{x_{TM}y}(y=d) = 0 \tag{17}$$

where the upper equation of (7) and the top one of (10) are used. By perceiving combined modal TE and TM fields as a collective whole, meaning that each modal group (or type) is regarded as a superposed entirety already encompassing all its component fields, but each sharing a common $e^{-jk_x^{univ}x}e^{-jk_z^{univ}z}$ phase term, the phase constants along the x and z directions parallel to the surface are universal, i.e., $k_x^{univ} = k_{x0}$ and $k_z^{univ} = k^{\text{above}}_{z_{TM}} = k^{\text{above}}_{z_{TE}}$ in order for phase continuity across the $y = d$ interface. Thus,

$$A^{\text{above}}_{TE}\frac{jk_z^{univ}}{\varepsilon_{abv}} + A^{\text{above}}_{TM}\frac{k_x^{univ}k^{\text{above}}_{y_{TM}}}{j\omega\mu_{abv}\varepsilon_{abv}} = 0. \tag{18}$$

Proceeding to (14), we require

$$E^{\text{groove}}_{z_{TE}y\,(p_{TE}=0)}(y=d) + E^{\text{groove}}_{z_{TM}y\,(p_{TM}=0)}(y=d) = E^{\text{above}}_{z_{TE}y}(y=d) + E^{\text{above}}_{z_{TM}y}(y=d) \tag{19}$$

in which the second term on the left-hand side vanishes [lower of (6)].

Using the upper equation of (3), the lower one of (7), and the bottom one of (10):

$$\sum_i A^{\text{groove}}_{TE}\frac{jk_{x0}}{\varepsilon_{\text{groove}}}e^{-jk_x^{univ}x}\sin\left(k^{\text{groove}}_{y_{TE}}d\right)e^{-jk_z^{univ}id_z} \underset{d_z\to 0}{\simeq} A^{\text{above}}_{TE}\frac{jk_{x0}}{\varepsilon_{abv}}e^{-jk_x^{univ}x}e^{-jk_z^{univ}z} - A^{\text{above}}_{TM}\frac{k^{\text{above}}_{y_{TM}}k_z^{univ}}{j\omega\mu_{abv}\varepsilon_{abv}}e^{-jk_x^{univ}x}e^{-jk_z^{univ}z} \tag{20}$$

where i is the groove index, noting how the left-hand side quantity varies with z in a stepwise manner, with each term of its summation being a piecewise constant within the i^{th} groove, i.e., $id_z - g/2 < z < id_z + g/2$.

Focusing within the i^{th} groove only, the summation over the groove index i in (20) is removed, resulting in

$$A^{\text{groove}}_{TE}\frac{jk_{x0}}{\varepsilon_{\text{groove}}}\sin\left(k^{\text{groove}}_{y_{TE}}d\right)e^{-jk_z^{univ}id_z} \underset{d_z\to 0}{\simeq} \left(A^{\text{above}}_{TE}\frac{jk_{x0}}{\varepsilon_{abv}} - A^{\text{above}}_{TM}\frac{k^{\text{above}}_{y_{TM}}k_z^{univ}}{j\omega\mu_{abv}\varepsilon_{abv}}\right) \times e^{-jk_z^{univ}z}\Big|_{id_z-\frac{g}{2}<z<id_z+\frac{g}{2}} \tag{21}$$

and as the period d_z tends to zero, the $e^{-jk_z^{univ}z}$ factor on the right-hand side of this (21) becomes approximately $e^{-jk_z^{univ}id_z}$, which is a constant within $id_z - g/2 < z < id_z + g/2$ (the i^{th} groove). This expresses that the continuous variation with z can be approximated as a piecewise discrete constant over the i^{th}

groove of nearly zero width. Hence, the resultant $e^{-jk_z^{univ}id_z}$ gets canceled out on both sides, leading to

$$A_{TE}^{\text{groove}}\frac{jk_{x0}}{\varepsilon_{\text{groove}}}\sin\left(k_{y_{TE}}^{\text{groove}}d\right)=A_{TE}^{\text{above}}\frac{jk_{x0}}{\varepsilon_{abv}}-A_{TM}^{\text{above}}\frac{k_{y_{TM}}^{\text{above}}k_z^{univ}}{j\omega\mu_{abv}\varepsilon_{abv}}. \quad (22)$$

Moving on to the final (15), we require

$$H^{\text{groove}}_{x_{TE}{}^{y}(p_{TE}=0)}(y=d)+H^{\text{groove}}_{x_{TM}{}^{y}(p_{TM}=0)}(y=d)=H^{\text{above}}_{x_{TE}{}^{y}}(y=d)+H^{\text{above}}_{x_{TM}{}^{y}}(y=d) \quad (23)$$

in which again the second term on the left-hand side vanishes [lower of (1)].

Using the upper equation of (4), the top equation of (9), and the upper one of (11),

$$\begin{aligned}&-\sum_i A_{TE}^{\text{groove}}\frac{k_{x0}k_{y_{TE}}^{\text{groove}}}{\omega\mu_{\text{groove}}\varepsilon_{\text{groove}}}e^{-jk_x^{univ}x}\\&\quad\times\cos\left(k_{y_{TE}}^{\text{groove}}d\right)e^{-jk_z^{univ}id_z}\\&\underset{d_z\to 0}{\simeq}-A_{TE}^{\text{above}}\frac{k_{x0}k_{y_{TE}}^{\text{above}}}{j\omega\mu_{abv}\varepsilon_{abv}}e^{-jk_x^{univ}x}e^{-jk_z^{univ}z}\\&\quad+A_{TM}^{\text{above}}\frac{jk_z^{univ}}{\mu_{abv}}e^{-jk_x^{univ}x}e^{-jk_z^{univ}z}.\end{aligned} \quad (24)$$

In the same way as for (20) and (21), we have

$$-A_{TE}^{\text{groove}}\frac{k_{x0}k_{y_{TE}}^{\text{groove}}}{\omega\mu_{\text{groove}}\varepsilon_{\text{groove}}}\cos\left(k_{y_{TE}}^{\text{groove}}d\right)=-A_{TE}^{\text{above}}\frac{k_{x0}k_{y_{TE}}^{\text{above}}}{j\omega\mu_{abv}\varepsilon_{abv}}+A_{TM}^{\text{above}}\frac{jk_z^{univ}}{\mu_{abv}}. \quad (25)$$

For surface-wave along the xz-plane surface of the corrugations, $k_{y_{TE}}^{\text{above}}$ and $k_{y_{TM}}^{\text{above}}$ are required to be imaginary, i.e.,

$$k_{y_{TE}}^{\text{above}}=-j\alpha_{y_{TE}}^{\text{above}}\quad\text{and}\quad k_{y_{TM}}^{\text{above}}=-j\alpha_{y_{TM}}^{\text{above}}. \quad (26)$$

The general formula for $k_{y_{TE}}^{\text{groove}}$ is given by

$$k_{y_{TE}}^{\text{groove}}=\sqrt{\omega^2\mu_{\text{groove}}\varepsilon_{\text{groove}}-\left(k_x^{univ}\right)^2-\left(k_z^{\text{groove}}\right)^2} \quad (27)$$

where k_z^{groove} is the phase constant along z in the groove region. But since $k_z^{\text{groove}}=0$ within each groove as $p_{TE}=p_{TM}=0$ under ACBC (presence of only dominant mode assumed), i.e.,

$$k_z^{\text{groove}}=\frac{p_{TE}\pi}{g}=\frac{p_{TM}\pi}{g}=0,\quad\text{under ACBC} \quad (28)$$

thus (27) reduces to (under ACBC)

$$k_{y_{TE}}^{\text{groove}}=\sqrt{\omega^2\mu_{\text{groove}}\varepsilon_{\text{groove}}-\left(k_x^{univ}\right)^2},\quad\text{under ACBC} \quad (29)$$

and due to the reason of collective whole mode sharing a common pair of surface wavenumber components: $k_{x0}=k_x^{univ}$ and k_z^{univ}, which together constituting a certain surface wave modal wavenumber

$$k_{surf}=\sqrt{\left(k_x^{univ}\right)^2+\left(k_z^{univ}\right)^2} \quad (30)$$

as explained just after (17) earlier, we may equate both modal (TE and TM) attenuation constants along the vertical y direction (perpendicular to the corrugation surface) for the upper half-space region above the corrugations, i.e.,

$$\alpha_{y_{TE}}^{\text{above}}=\alpha_{y_{TM}}^{\text{above}}\underset{say}{=}\alpha_y^{\text{above}} \quad (31)$$

$$\text{with}\ \left(\alpha_y^{\text{above}}\right)^2=\left(k_x^{univ}\right)^2+\left(k_z^{univ}\right)^2-\omega^2\mu_{abv}\varepsilon_{abv} \quad (32)$$

where α_y^{above} is positive real.

D. Transcendental Characteristic Equations

The three pertinent equations are (18), (22) and (25), and the three unknowns are A_{TE}^{groove}, A_{TE}^{above}, and A_{TM}^{above}, which may be cast into a 3×3 matrix system. By setting the matrix determinant to zero for nontrivial solutions, we obtain the following characteristic equation:

$$\begin{aligned}&\mu_{\text{groove}}\left\langle k_{\text{above}}^2\left(k_z^{univ}\right)^2-\left(k_x^{univ}\right)^2\left[\left(k_x^{univ}\right)^2+\left(k_z^{univ}\right)^2-k_{\text{above}}^2\right]\right\rangle\cdots\\&\quad\times\left\{\tan\left[d\sqrt{k_{\text{groove}}^2-\left(k_x^{univ}\right)^2}\right]\right\}/\sqrt{k_{\text{groove}}^2-\left(k_x^{univ}\right)^2}\\&=\mu_{abv}\left[\left(k_x^{univ}\right)^2+\left(k_z^{univ}\right)^2\right]\\&\quad\times\sqrt{\left(k_x^{univ}\right)^2+\left(k_z^{univ}\right)^2-k_{\text{above}}^2}\end{aligned} \quad (33)$$

where

$$k_{\text{groove}}=2\pi f\sqrt{\mu_{\text{groove}}\varepsilon_{\text{groove}}};\quad k_{\text{above}}=2\pi f\sqrt{\mu_{abv}\varepsilon_{abv}}. \quad (34)$$

Depending on which two of the following three quantities: 1) frequency $f=\omega/(2\pi)$, 2) k_x^{univ}, and 3) k_z^{univ}, are *a priori* prefixed as known values, the third quantity remains as the only unknown in this (33), which may then be solved for as roots of this characteristic equation. Doing so yields the required information for plotting various path-regions of the dispersion diagram.

E. Solution of Matrix Equation for Amplitude Coefficients

Equations (18), (22), and (25) may be cast into the following matrix equation:

$$\begin{bmatrix}M_{11}&M_{12}&M_{13}\\M_{21}&M_{22}&M_{23}\\M_{31}&M_{32}&M_{33}\end{bmatrix}\begin{bmatrix}A_{TE}^{\text{groove}}\\A_{TE}^{\text{above}}\\A_{TM}^{\text{above}}\end{bmatrix}=\begin{bmatrix}0\\0\\0\end{bmatrix} \quad (35)$$

where the matrix elements M_{ij} need no further specification.

By performing Gauss elimination, the following is obtained:

$$\begin{bmatrix}A_{TE}^{\text{groove}}\\A_{TE}^{\text{above}}\\A_{TM}^{\text{above}}\end{bmatrix}=\begin{bmatrix}x_1\\x_2\\x_3\end{bmatrix}=x_3\begin{bmatrix}\frac{(M_{22}M_{13}-M_{12}M_{23})}{(M_{12}M_{21})}\\-M_{13}/M_{12}\\1\end{bmatrix} \quad (36)$$

in which $x_3=A_{TM}^{\text{above}}$ is any arbitrary scaling amplitude. All M_{ij} matrix elements would have become fully evaluatable upon solving the characteristic equation of (33) for either the phase constant (k_x^{univ} or k_z^{univ}) or frequency of interest, and by substituting these A_{TE}^{groove}, A_{TE}^{above}, and A_{TM}^{above} into (1)–(11), the com-

plete closed-form analytical expressions of the fields in both the groove region and the half-space above the corrugations may be obtained as mathematical functions of all geometrical and material parameters of the corrugated structure.

F. Consistency With Modal Surface Impedances and Input Impedance of Shorted Transmission Line

The surface impedance looking down at $y = d$ towards the PEC floor of the corrugations are defined as follows:

$$Z_{s\downarrow}^{\overset{TE}{groove}} = -\frac{E_{z_{TE^y}}^{\text{groove}}(y=d)}{H_{x_{TE^y}}^{\text{groove}}(y=d)} = j\frac{\omega\mu_{\text{groove}}}{k_{y_{TE}}^{\text{groove}}}\tan\left(k_{y_{TE}}^{\text{groove}}d\right) \tag{37}$$

where $\omega\mu_{\text{groove}}/k_{y_{TE}}^{\text{groove}}$ is the familiar TE^y modal impedance Z_c^{TE}, therefore yielding the familiar input impedance of a shorted transmission line of length d and characteristic impedance Z_c^{TE}.

Similarly, the input impedances looking at $y = d$ interface upwards into the upper half-space region for the two modal groups are

$$\begin{aligned} Z_{s\uparrow}^{\overset{TE}{above}} &= -\frac{E_{x_{TE^y}}^{\text{above}}(y=d)}{H_{z_{TE^y}}^{\text{above}}(y=d)} = \frac{E_{z_{TE^y}}^{\text{above}}(y=d)}{H_{x_{TE^y}}^{\text{above}}(y=d)} \\ &= \frac{j\omega\mu_{abv}}{\sqrt{(k_x^{univ})^2+(k_z^{univ})^2-k_{\text{above}}^2}} = \frac{j\omega\mu_{abv}}{\gamma_y^{\text{above}}} \end{aligned} \tag{38}$$

being the familiar TE modal impedance, whereas

$$\begin{aligned} Z_{s\uparrow}^{\overset{TM}{above}} &= -\frac{E_{x_{TM^y}}^{\text{above}}(y=d)}{H_{z_{TM^y}}^{\text{above}}(y=d)} = \frac{E_{z_{TM^y}}^{\text{above}}(y=d)}{H_{x_{TM^y}}^{\text{above}}(y=d)} \\ &= \frac{\sqrt{(k_x^{univ})^2+(k_z^{univ})^2-k_{\text{above}}^2}}{j\omega\varepsilon_{abv}} = \frac{\gamma_y^{\text{above}}}{j\omega\varepsilon_{abv}} \end{aligned} \tag{39}$$

being the familiar TM modal impedance

G. Refinement Factor via Period to Groove-Width Ratio

From Section II-F, $Z_{s\uparrow}^{\overset{TE}{above}}$ and $Z_{s\uparrow}^{\overset{TM}{above}}$ of (38) and (39) were the impedances looking upwards into the upper half-space region above the corrugations. The E_x and E_z in the numerators of the expressions for these impedances are E-field components that are tangential to the corrugation surface and which vanish over the top PEC surfaces of the metallic ridges. Before proceeding further, it is first emphasized that the rightmost sides of both (38) and (39), being the well-known classical expressions for the TE and TM modal impedances of a medium with parameters $(\varepsilon_{abv}, \mu_{abv})$ for propagation along y, must always hold and stay unchanged (there is no reason for these impedances to be altered). Hence, it may be hypothesized that the tangential $E_{x_{T\zeta^y}}^{\text{above}}$ and $E_{z_{T\zeta^y}}^{\text{above}}$ field components (ζ either E or M), **but only** on the corrugation surface: $y = d$, may be corrected by an *incremental* (>1) factor d_z/g, where d_z is the corrugation period (see Fig. 1 again) and g is the groove-width. In this way, a multiplication of these correctively magnified $E_{x_{T\zeta^y}}^{\text{above}}$ and $E_{z_{T\zeta^y}}^{\text{above}}$ fields on the corrugation surface with the *reduction* (<1) factor g/d_z (as required by the fractional existence of the upper region's tangential E-field components over only the apertures of the grooves, but vanishing over the ridge-tops), *neutralizes* that aforementioned incremental factor, thereby *maintaining* the TE and TM modal impedances looking upwards into the upper half-space region $(\varepsilon_{abv}, \mu_{abv})$ above the corrugations, which must be preserved as explained earlier. However, this correction factor, $d_z/g > 1$ applies only to the tangential (E_x, E_z) components and *only just over* the surface $(y = d)$.

To mathematically convey these textual descriptions, the following corrected tangential field components are defined:

$$E_{w_{T\zeta^y}}^{\overset{above}{correc}}(y=d) = \frac{d_z}{g}E_{w_{T\zeta^y}}^{\text{above}}(y=d) \tag{40}$$

in which w denotes either x or z. The script *correc* signifies *corrected* and ζ represents E or M as before. The right-side field quantity is that of the original ones in (7) and the top and bottom of (10). Notice the explicit evaluation at $y = d$ to stress the validity of this correction only over the surface. Subsequently, these corrected tangential electric field components are used for the numerators of the surface impedance [those of (38) and (39)]:

$$Z_{s\uparrow}^{\overset{T\zeta}{above}} = -\frac{\frac{g}{d_z}E_{x_{T\zeta^y}}^{\overset{above}{correc}}(y=d)}{H_{z_{T\zeta^y}}^{\text{above}}(y=d)} = \frac{\frac{g}{d_z}E_{z_{T\zeta^y}}^{\overset{above}{correc}}(y=d)}{H_{x_{T\zeta^y}}^{\text{above}}(y=d)} \tag{41}$$

noting the reduction factor g/d_z as explained. Substituting in (40) yields back exactly the same ones as (38) and (39), thereby maintaining their rightmost classical expressions: $j\omega\mu_{abv}/\gamma_y^{\text{above}}$ and $\gamma_y^{\text{above}}/j\omega\varepsilon_{abv}$ as required. Therefore, what this (41) says is that the upward-looking surface impedance involving tangential electric field components at $y = d$ effectively uses the *uncorrected* tangential E-fields also at $y = d$ given by the original expressions of (7) and the top and bottom of (10), thus appropriately preserving (38) and (39).

As such, the key concepts are as follow. The upward surface impedance [(38), (39) or (41) combined] involves tangential fields of the upper half-space region as a collective whole throughout the entire surface, since indeed the entire upper half-space may be perceived as a transmission line for propagation along the vertical y direction. The nullification of the tangential electric field components of the upper half-space across the metallic ridges through the reduction factor of g/d_z is thus required. On the other hand, the four ACBC relations (12)–(15) are all satisfied individually over each groove aperture, in an element-by-element fashion [see (20) and (21)]. Hence, the tangential electric field components of the upper half-space region used in these boundary conditions are exempted from this reduction factor. However, they must use the corrected form of (40) evaluated at $y = d$. In other words, it is these amended tangential electric fields over this interface that are used in the ACBC equations (indeed involving only tangential field components parallel to the corrugated surface). Subsequently, since the ultimate characteristic equation of (33) is derived from these rectified ACBC relations, the correction factor thus shows up in this transcendental relation (33), i.e., is translated to it (see the ultimate corrected version of (44) later).

However, it is noted that no such correction factor is required of the fields within the grooves. This is because their constrained existence by mathematical definition of (1) to (6) already ensures that they prevail just exactly over the aperture of the grooves. Hence, the groove-aperture fields used in

(37) for the surface impedance looking downward towards the PEC-shorted end (floor) of the TEM-type parallel-plate transmission line modeling the grooves, which also must not be altered [i.e., the extreme right-hand side of (37)], do not need any adjustment in amplitude, since no reduction of tangential electric fields across PEC ridges is entailed, unlike the fields in the upper-half space above the corrugations.

In order to implement this refinement, the characteristic equation obtained by equating the system matrix determinant to zero as done in Section II-D has to be re-derived.

The three pertinent equations (18), (22), and (25) were, respectively, from (17), (19), and (23), of which only the former two involves E^{above} terms whereas the latter equation does not contain any of them. Since the correction factor d_z/g needs only be applied to the E^{above} field terms, only (17) and (19) require amendment. However, it can be easily seen that this multiplicative correction factor would get canceled throughout (17), leaving it unchanged. Therefore, the only change required would be of (19), which becomes

$$E^{\text{groove}}_{z_{TE^y}}(y=d) = \frac{d_z}{g}\left[E^{\text{above}}_{z_{TE^y}}(y=d) + E^{\text{above}}_{z_{TM^y}}(y=d)\right]. \tag{42}$$

Consequently, only (22) needs to be amended to become

$$A^{\text{groove}}_{TE}\frac{jk_{x0}}{\varepsilon_{\text{groove}}}\sin\left(k^{\text{groove}}_{y_{TE}}d\right) - A^{\text{above}}_{TE}\frac{d_z}{g}\frac{jk_{x0}}{\varepsilon_{abv}} + A^{\text{above}}_{TM}\frac{d_z}{g}\frac{k^{\text{above}}_{y_{TM}}k^{univ}_z}{j\omega\mu_{abv}\varepsilon_{abv}} = 0. \tag{43}$$

As a result, M_{22} and M_{23} have to modified by including now the multiplicative correction factor d_z/g to each of them. The system matrix determinant shall then also be amended, leading to the following corrected characteristic equation that takes into account the effects of non-negligible ridge-width to period ratio:

$$\begin{aligned}\mu_{\text{groove}}&\left\langle k^2_{\text{above}}\left(k^{univ}_z\right)^2 - \left(k^{univ}_x\right)^2\left[\left(k^{univ}_x\right)^2 + \left(k^{univ}_z\right)^2 - k^2_{\text{above}}\right]\right\rangle \cdots \\ &\times\left\{\tan\left[d\sqrt{k^2_{\text{groove}} - \left(k^{univ}_x\right)^2}\right]\right\} \Big/ \sqrt{k^2_{\text{groove}} - \left(k^{univ}_x\right)^2} \\ &= \frac{d_z}{g}\mu_{abv}\left[\left(k^{univ}_x\right)^2 + \left(k^{univ}_z\right)^2\right] \\ &\times\sqrt{\left(k^{univ}_x\right)^2 + \left(k^{univ}_z\right)^2 - k^2_{\text{above}}}.\end{aligned} \tag{44}$$

Hence, note that the correction factor only amends the characteristic equation so that it represents a more accurate dispersion relation (as will be demonstrated later) and provides a better matrix solution for the modal amplitude coefficients [see (35) and (36)]. It however should neither appear in (7) nor the top and bottom relations of (10) representing the tangential E-fields as a function of general spatial coordinates, since this factor is valid only over the surface $(y = d)$ but not anywhere else.

III. Transverse Resonance Technique

In this section, the transverse resonance technique (TRT) for deriving the transcendental characteristic equation for the planar corrugated surface shall be presented.

A. TM^y Modes

According to the TRT, the surface impedance "looking" downwards towards the corrugated surface must equal that "looking" upwards into the upper half-space, i.e.

$$Z^{\overset{TE}{groove}}_{s\downarrow} = Z^{\overset{TM}{abv}}_{s\uparrow} \tag{45}$$

noting the TM^y nature of the modal impedance 'looking' upwards on the right-hand side, whereas the modal type on the left-hand side is TE since there can only be TE modes within the grooves under ACBC. Using (37) and (39) for the left and right hand side quantities, we have

$$j\frac{g}{d_z}\frac{\omega\mu_{\text{groove}}}{k^{\text{groove}}_{y_{TE}}}\tan\left(k^{\text{groove}}_{y_{TE}}d\right) = \frac{\gamma^{abv}_y}{j\omega\varepsilon_{abv}} = \frac{\sqrt{k^2_z + k^2_x - k^2_{abv}}}{j\omega\varepsilon_{abv}} \tag{46}$$

noticing the averaging factor g/d_z for the impedance "looking" down into the grooves on the left-hand side, and where

$$k^{\text{groove}}_{y_{TE}} = \sqrt{k^2_{\text{groove}} - k^2_x} \tag{47}$$

since $k_z = 0$ inside the grooves (cavities), and with

$$k_{abv} = 2\pi f\sqrt{\mu_{abv}\varepsilon_{abv}} \text{ and } k_{\text{groove}} = 2\pi f\sqrt{\mu_{\text{groove}}\varepsilon_{\text{groove}}}. \tag{48}$$

The abv scripts denote "above," meaning the upper-half free-space above the corrugations.

Upon squaring both sides of (46), k_z can be expressed as

$$k_z = \sqrt{k^2_{abv} - k^2_x + \left(\frac{g}{d_z}\right)^2\frac{\left(\omega^2\mu_{\text{groove}}\varepsilon_{abv}\right)^2}{k^2_{\text{groove}} - k^2_x}\tan^2\left(d\sqrt{k^2_{\text{groove}} - k^2_x}\right)} \tag{49}$$

which, for a certain pair of fixed (k_z, k_x) values, can be solved for the frequency f as roots, manifested within $\omega = 2\pi f$ and the two wavenumbers k_{abv} and k_{groove} given by (48). As this (k_z, k_x) in turn pertains to a certain surface-wavenumber:

$$k_{surf} = \sqrt{k^2_z + k^2_x} \tag{50}$$

meaning that each such k_{surf} has its corresponding resonant f detected as roots, the graph of f versus k_{surf} may be generated, being the dispersion diagram.

B. TE^y Modes

In a similar fashion as TM^y modes, the surface-wavenumber for nonzero phi angle of grazing propagation on the corrugated surface can be derived by the TRT. Doing so, we obtain

$$Z^{\overset{TE}{cav}}_{s\downarrow} = Z^{\overset{TE}{abv}}_{s\uparrow}$$

which upon using (37) and (38), yields

$$j\frac{g}{d_z}\frac{\omega\mu_{\text{groove}}}{k^{\text{groove}}_{y_{TE}}}\tan\left(k^{\text{groove}}_{y_{TE}}d\right) = \frac{j\omega\mu_{abv}}{\gamma^{abv}_y} = \frac{j\omega\mu_{abv}}{\sqrt{k^2_z + k^2_x - k^2_{abv}}}$$

$$\Rightarrow \underbrace{k_z^2 + k_x^2}_{k_{surf}^2} = \left[\frac{\mu_{abv} k_{y_{TE}}^{\text{groove}}}{\left(\frac{g}{d_z}\right)\mu_{\text{groove}} \tan\left(k_{y_{TE}}^{\text{groove}} d\right)}\right]^2 + k_{abv}^2 \quad (51)$$

noticing again the averaging factor g/d_z for the impedance, and where

$$k_{y_{TE}}^{cav} = \sqrt{k_{\text{groove}}^2 - k_x^2} \quad (52)$$

since $k_z = 0$ may be approximated inside the grooves (cavities) to good accuracy, and with k_{abv} and k_{groove} as of (48).

Hence, in the same way as (49), (51) may be solved for the frequency f as roots for a certain fixed (k_x, k_y).

IV. Numerical Results and Discussion

A. Dispersion Diagrams

Here, we shall present the dispersion diagrams for the conventionally named "O → X" path of the typical y-directed corrugations having periodicity along x (the xy plane is parallel to the corrugated surface), being actually O → Z path here for the present axis configuration with z periodicity, as shown in Fig. 1. For this "O → X" case (O → Z here), $k_{x0} = k_x^{univ}$ is set to zero. Subsequently, the graph of f versus k_z^{univ} shall be generated, the latter being the solved roots obtained repeatedly for every frequency considered. For this case, instead of numerical root-solving, the dispersion equation may be cast into a cubic form, whose roots can then be obtained via the analytic formulas. The dispersion diagrams generated by the present ACBC-based method are compared with those obtained from **two full-wave validating tools**: a commercial full-wave simulator software: CST Microwave Studio, as well as an independent self-developed computer program code [20] based on full-wave modal analysis with the method of moments using parallel-plate waveguide (PPW) cavity Green's functions (GF) and a numerical Green's function for stratified media called G1DMULT. Two arbitrary examples shall be studied as follow.

1) First Arbitrary Example—Comparison with Moment Method: For this so-called first arbitrary example, the parameters are as follow: period $d_z = 2$ mm, groove-width $g = 0.85^* d_z$, iris width $= 0.75g$, depth $d = 8$ mm, $\varepsilon_{\text{rel,groove}} = 2$; $\mu_{\text{rel,groove}} = 1$.

The "O → X" (O → Z here) dispersion for this case is shown in Fig. 2, obtained by the present ACBC-based method (shown as lines with cross-type markers) and compared with that generated by the moment method code.

As seen, the roots of the characteristic equation (33) produce a dispersion trace which takes on the form of cyclic "peaking" of the k_z^{univ} (horizontal axis) at various resonant frequencies. Moreover, the trace just "grazes" the light-line, i.e., it is tangent to it, occurring at frequencies slightly above those whereby the trace has dropped back to its local minima (of the horizontal axis value) and begun to rise again. However, as observed, only the rising parts of the "peaking" trace after the "grazing" are relevant, for which the agreement with the dispersion trace generated by the full-wave moment method code is seen to be superb. In fact, they agree so well that the traces are virtually indistinguishable.

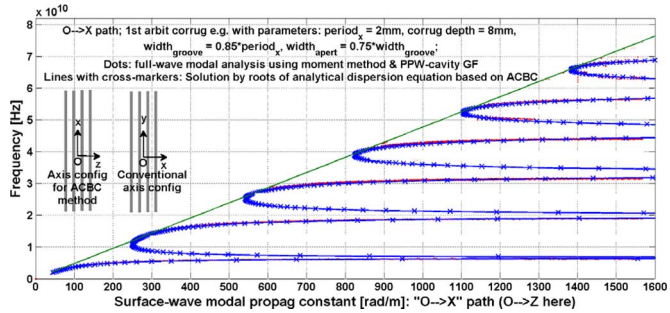

Fig. 2. "O → X" (O → Z here) dispersion for first corrugation example—ACBC method compared with full-wave moment method [20].

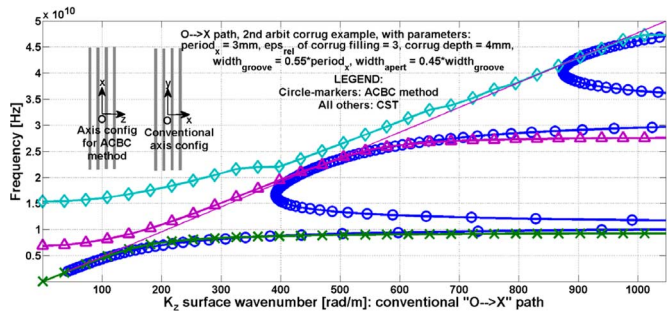

Fig. 3. "O → X" (O → Z here) dispersion for second corrugation example—ACBC method (circle markers) compared with commercial solver CST (all other marker-types).

An interesting aspect is now pointed out. The frequencies at which the peaks occur coincide perfectly with the so-called "soft" frequencies [11] of the corrugations, defined as

$$f_n^{\text{soft}} = \frac{c(2n+1)}{(4d_{\text{soft}}\sqrt{\varepsilon_{\text{rel,groove}}})} \quad (53)$$

where n is an integer (includes zero) representing the order of the soft boundary condition, c is the speed of light in vacuum, d_{soft} is the depth of the corrugations at which the soft boundary condition holds, being simply the groove depth d, and $\varepsilon_{\text{rel,groove}}$ is the relative permittivity of the dielectric filling the grooves.

2) Second Arbitrary Example—CST Comparison: For this so-called second arbitrary example, the parameters are as follow: period $d_z = 3$ mm, groove-width $g = 0.55^* d_z$, iris width $= 0.45g$, depth $d = 4$ mm, $\varepsilon_{\text{rel,groove}} = 3$; $\mu_{\text{rel,groove}} = 1$.

This time, a comparison is made with the other validator the commercial full-wave solver: CST, as shown in Fig. 3. Evidently, the agreement is again seen to be excellent.

As additional results and still on this second example, in order to demonstrate the efficacy of this ACBC method for not only the principal direction of surface-wave propagation, but for oblique directions as well, the dispersion graphs for one other path of the typical "O → X → M → Y → O" dispersion diagram typical of two-dimensional periodic electromagnetic bandgap (EBG) structures is given in Fig. 4 providing the "X → M" portion (Z → M here). However, for the present case of corrugations, there is actually no periodicity in the

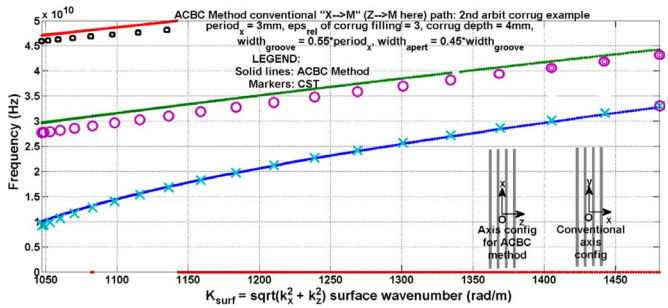

Fig. 4. "X → M" (Z → M here) dispersion for second corrugation example—ACBC method (solid traces) compared with commercial solver CST (markers).

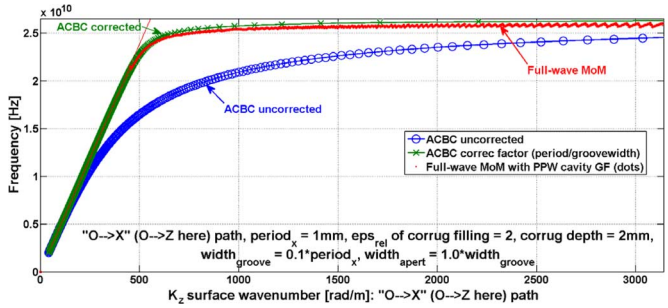

Fig. 5. "O → X" (O → Z here) dispersion diagram, for $\boldsymbol{g = 0.1d^z}$. Uncorrected [eq. (33)] and corrected [eq. (44)] ACBC methods compared with full-wave moment method [20], for $d_z = 1$ mm, $\varepsilon_{\mathrm{rel,groove}} = 2$, $d = 2$ mm.

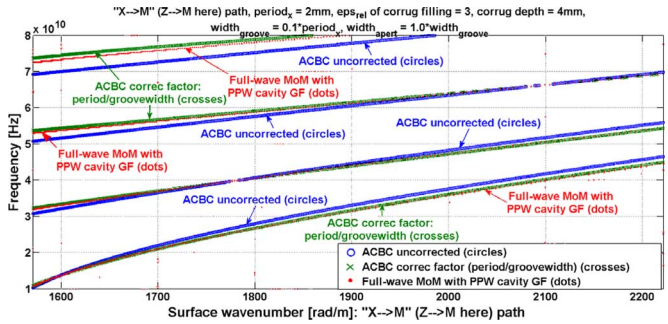

Fig. 6. "X → M" (Z → M here) dispersion diagram, for $\boldsymbol{g = 0.1d^z}$. Uncorrected [eq. (33)] and corrected [eq. (44)] ACBC methods compared with full-wave moment method [20], for $d_z = 2$ mm, $\varepsilon_{\mathrm{rel,groove}} = 3$, $d = 4$ mm.

direction (x here) along them. Nonetheless, we shall still set the Brillouin limit along this direction as π divided by the same period (along z) of the corrugations, thus assuming a square unit cell (although strictly, the unit cell is an infinitely long strip in the zx plane of the corrugations, infinitely long along x, the orientation of the corrugations). Doing this is merely out of adhering with the procedure in the validating software CST for treating typically two-dimensionally periodic structures rather than of any scientific basis. The comparison between the present ACBC method and CST for Fig. 4 again demonstrates fine agreement.

3) Refinement Factor for Accuracy Improvement: Especially for Small Groove-Width to Period Ratios: We now present the results of including the correction factor in the characteristic equation conveyed by (44), thereby exemplifying its importance.

"O → X" path (O → Z here)

The O → Z path of the dispersion diagram is studied first. A wide assortment of cases spanning over three parameters has been thoroughly simulated, both by the present ACBC method [using the uncorrected (33) and corrected (44)] and the self-developed full-wave moment method code [20], for $g/d_z = 0.1$ (being a particularly small value) and with $\mu_{\mathrm{rel,groove}} = 1$ universal throughout. The investigated parameters are i) the period ($d_z = 1$ mm, 2 mm & 3 mm), ii) the groove relative permittivity ($\varepsilon_{\mathrm{rel,groove}}$ =2 to 7 in unit steps), and iii) the corrugation depth ($d = 2$ mm to 7 mm in unit mm steps). Due to obvious space limitations, the dispersion diagram for only one randomly selected case amongst the large $3 \times 6 \times 6$ parametric space can be presented. The sub-case chosen for presentation pertains to $d_z = 1$ mm, $\varepsilon_{\mathrm{rel,groove}} = 2$, $d = 2$ mm, whose dispersion diagram is given in Fig. 5. As clearly evident, the correction factor d_z/g in the characteristic equation of (44) indeed significantly improves the accuracy of the ACBC method without any correction factor.

"X → M" path (Z → M here)

The results for oblique directions of surface-wave propagation are now given, i.e., the Z → M path of the dispersion diagram (the "X → M" according to usual convention when the horizontal periodicity is along x). As was for the preceding O → Z path, the solutions for a diverse range of parametric cases had been generated, by the present ACBC method [using the uncorrected (33) and corrected (44)] and the full-wave moment method code, but again due to space constraints, only one dispersion diagram shall be provided by Fig. 6 pertaining to an arbitrarily chosen case with parameters: $g/d_z = 0.1$, $d_z = 2$ mm, $\varepsilon_{\mathrm{rel,groove}} = 3$, and $d = 4$ mm. Evidently, the correction factor d_z/g in (44) again considerably enhances the correctness of the ACBC method for treating oblique surface-wave propagation as compared with the case without any correction factor.

TABLE I
CPU TIMES FOR DISPERSION-DIAGRAM PROPERTIES BY THREE METHODS

CST [s]		17,233
Moment Method [s]		15,079
ACBC [s]	O→Z	2.23
	Z→M	4.27

4) Comparison of Processor Times Between ACBC and Full-Wave Solvers (CST and Moment Method): Table I tabulates the CPU processing times taken up for acquisition of the dispersion graph for the "O → X" path (O → Z here) for that same second corrugation example (of Section IV-A2) by all three methods: i) CST, ii) the moment method, and iii) the ACBC method. The same number of data points in the band-diagram generated by all three tools is considered for fairness of comparison. As seen, both CST and the moment method clock over 15 000 seconds (17 233 and 15 079 seconds, respectively), whereas the ACBC approach requires only just 2.23 seconds, a 7725-fold reduction in CPU time compared to CST and a 6760-times mitigation when up against the moment method code.

Even when the dispersion diagram for oblique azimuth angles of surface-wave propagation is the subject of comparison, i.e., for the "X → M" (Z → M here) path, the generation of which

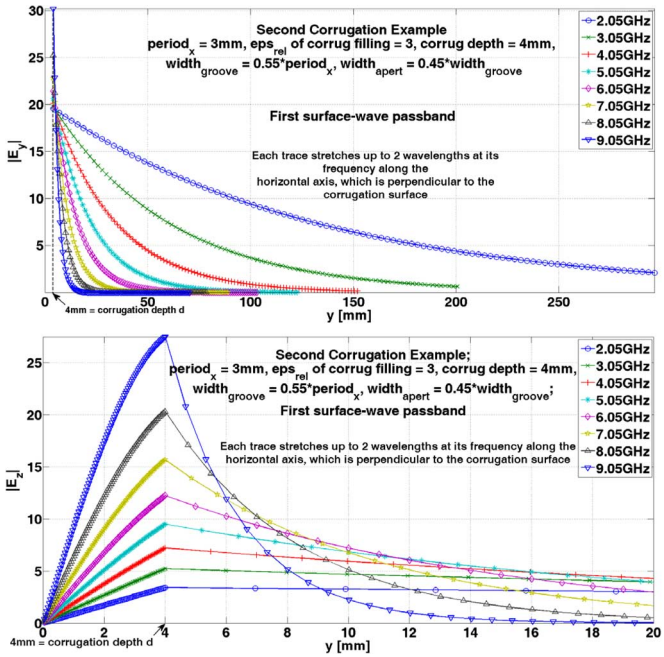

Fig. 7. Magnitude of E-field components plotted against vertical y direction, for several frequencies within the **first** surface wave passband (0 to 10 GHz). Upper: $|E_y|$ and lower: $|E_z|$.

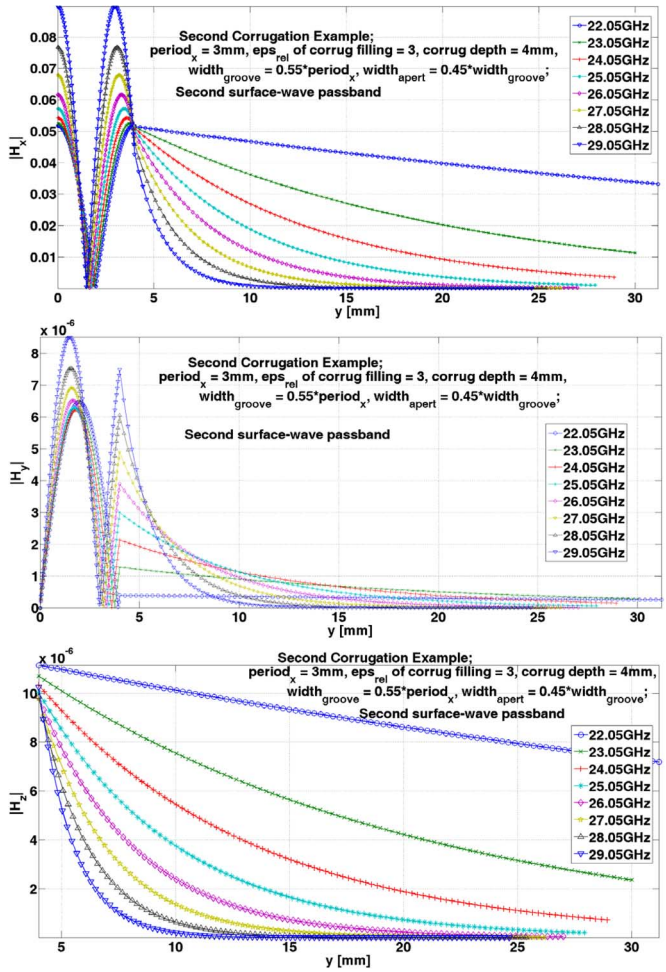

Fig. 8. Magnitude of H-field components plotted against vertical y direction, for several frequencies within the **second** surface wave passband (22 to 30 GHz).

by ACBC requiring a numerical search for roots rather than direct evaluation of formulaic roots of cubic equations as would had been possible with the principal direction (the O $\rightarrow$ X path), the CPU time taken by the ACBC method is only slightly longer, being just 4.274 seconds, which is still an immensely shorter duration than either CST or the moment method (also as seen from Table I).

B. Field Distributions

The mesh-plots of the fields as mentioned at the end of Section II-E are now provided for the second arbitrary example of Section IV-A2. Fig. 7 shows the variation of the magnitude of the E-field components with the vertical y-direction for various frequencies within the first surface wave passband (0 to 10 GHz according to Fig. 3), whereas the graphs of Fig. 8 are for the H-field components within the second surface-wave passband from 22 to 30 GHz. As the frequency rises and moves deeper into the first surface-wave regime (2.05 through 9.05 GHz in 1-GHz steps, as selected for plotting), the corresponding increased surface-wave phase constant k_z^{univ} beyond $k_{\text{above}} = \omega\sqrt{\mu_{abv}\varepsilon_{abv}}$ and thus strengthened attenuation constant α_y^{above} along the vertical y direction [see (32), with $k_x^{univ} = 0$] is indeed demonstrated by the progressively steepened exponential decay of the various field components with increasing frequency. In addition, the continuity of the tangential $|E_z|$, $|H_x|$ and $|H_y|$ components across the $y = d$ interface between the corrugations and the upper half region is observed for all frequencies within both surface-wave passbands, as required.

The closed-form analytical field expressions that yield these graphs offer important prospects of being used in the modal analysis of such planar corrugated surfaces in coexistence with other microwave structures, such as mode-matching with waveguides, and even facilitate calculations of radiation from apertures of surface-wave antennas composed of corrugations.

The fact that these field expressions are obtainable by this ACBC method puts it on par with full-wave solvers known for this same ability, one which the TRT lacks. Yet, the ACBC method surpasses full-wave solvers in terms of speed, as the previous subsection has shown.

V. Comparison With TRT

A. TM^y Modes

By solving (49) for the frequency f as roots and then plotting against the corresponding k_{surf} given by (50) as prescribed earlier for an arbitrary case of corrugations: $d_z = 3$ mm, $\varepsilon_{\text{rel,groove}} = 3$, $d = 4$ mm, $g = 2.25$ mm, and for a fixed oblique azimuth phi angle of surface-wave propagation direction: $\phi = 30°$ (measured from the z-axis towards the y-axis), the comparison between the dispersion diagram obtained by (49) with those generated by our ACBC approach using (44) as well as the self-developed full-wave moment method code [20] serving as the supreme check is given in Fig. 9. As observed, our ACBC method provides higher accuracy than the TRT. It is noted that both these methods have the correction factor (d_z/g

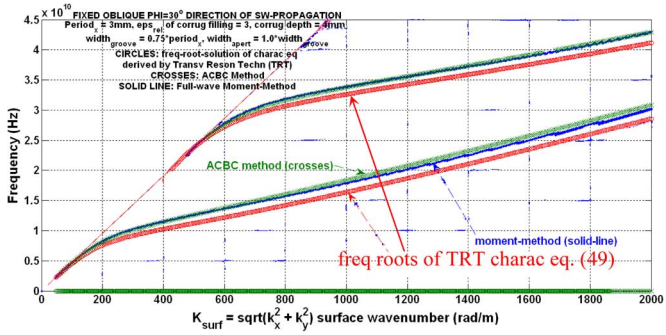

Fig. 9. Comparison between moment method, ACBC approach of (44) and TRT-derived Eq. (49) for TM^y polarization; for fixed oblique phi $= 30°$ angle of surface-wave propagation direction (measured from z toward x axis), for $d_z = 3$ mm, $\varepsilon_{\mathrm{rel,groove}} = 3$, $d = 4$ mm, $g = 2.25$ mm.

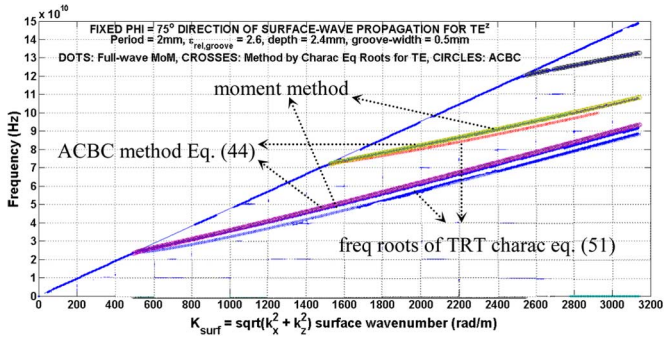

Fig. 10. Comparison between moment method, ACBC approach of eq. (44) and TRT-derived eq. (51) for TE^y polarization, for fixed oblique phi $= 75°$ angle of surface-wave propagation direction (measured from z toward x axis), for $d_z = 2$ mm, $\varepsilon_{\mathrm{rel,groove}} = 2.6$, $d = 2.4$ mm, $g = 0.5$ mm.

for ACBC, g/d_z for TRT) incorporated and thus are compared fairly on a common basis.

B. TE^y Modes

Likewise for TE^y modes, the efficacy of (51) shall be tested for the arbitrary case of $\phi = 75°$ (as before, measured from the z towards x axis) For another random set of parameters: $d_z = 2$ mm, $\varepsilon_{\mathrm{rel,groove}} = 2.6$, $d = 2.4$ mm, $g = 0.5$ mm, and $\phi = 75°$ as stated, Fig. 10 provides a comparison between the dispersion diagrams obtained by the full-wave moment method (serving as the check), the ACBC method via (44), and the TRT-derived characteristic equation (51) for TE^y mode. Evidently, the accuracy of the ACBC approach is again seen to be notably higher than that of the TRT.

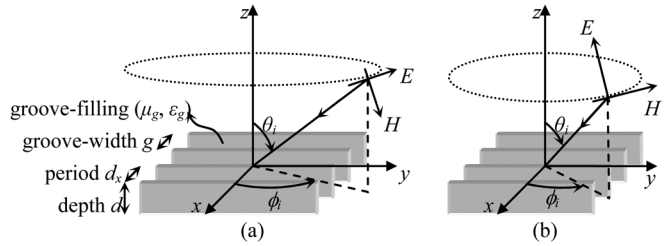

Fig. 11. (a) TE^z polarized plane wave. (b) TM^z polarized plane wave.

VI. Reflection Analysis for Oblique Azimuth Planes of Incidence (Nonzero Incident PHI)

A. TE^z Polarized Incidence

Consider now, the y-directed corrugations lying in the xy plane illuminated by a TE^z polarized incident plane wave as shown in Fig. 11(a). The medium parameters are (μ_i, ε_i) with associated wave impedance $\eta_i = \sqrt{(\mu_i/\varepsilon_i)}$ and wavenumber $k_i = 2\pi f\sqrt{(\mu_i\varepsilon_i)}$.

The fields of this plane wave are stated as

$$\vec{E}^i_{TE^z} = E_0(-\hat{x}\sin\phi_i + \hat{y}\cos\phi_i)e^{j\left(k_{x_i}x+k_{y_i}y+k_{z_i}z\right)} \tag{54}$$

$$\begin{aligned}\vec{H}^i_{TE^z} &= \frac{1}{\eta_i}\left(\hat{r}^i \times \vec{E}^i_{TE^z}\right)\\ &= \frac{E_0}{\eta_i}\begin{pmatrix}-\sin\theta_i\cos\phi_i\\ \sin\theta_i\sin\phi_i\\ -\cos\theta_i\end{pmatrix}\\ &\quad\times\begin{pmatrix}-\sin\phi_i\\ \cos\phi_i\\ 0\end{pmatrix}e^{j\left(k_{x_i}x+k_{y_i}y+k_{z_i}z\right)}\end{aligned} \tag{55}$$

where

$$k_{x_i} = k_i\sin\theta_i\cos\phi_i,\ k_{y_i} = k_i\sin\theta_i\sin\phi_i,\ \text{and}\ k_{z_i} = k_i\cos\theta_i. \tag{56}$$

Extracting just the $\mathrm{TE}_{\phi=90}$ components in the $\Pi = 90°$ (yz) plane: E_x, H_y and H_z, we write the following, as shown at the bottom of the page, noting the appending exponential terms representing unusual phasing along the x-direction, thus being unlike typical plane-waves propagating within the yz plane, i.e., a TE^z-polarized plane-wave (x-directed E-field) propagating in the $phi_i = 90°$ (yz) plane but with an unusual phase variation along x.

$$\vec{E}^i_{TE^z_{\phi=90}} = \underbrace{\hat{x}(-E_0\sin\phi_i)e^{j\left(k_{y_i}y+k_{z_i}z\right)}}_{\substack{\text{usual } x-\text{directed } E-\text{field of TE}^z \text{ polarized}\\ \text{plane-wave in } \phi_i=90° \text{ plane}}}\ \underbrace{e^{jk_{x_i}x}}_{\substack{unusually\\ phased\\ along\ x}} \tag{57}$$

$$\vec{H}^i_{TE^z_{\phi=90}} = \underbrace{\frac{E_0}{\eta_i}(\hat{y}\cos\theta_i\sin\phi_i - \hat{z}\sin\theta_i)e^{j\left(k_{y_i}y+k_{z_i}z\right)}}_{\text{usual } yz-\text{directed } H-\text{field of TE}^z \text{ polarized plane-wave in } \phi_i=90° \text{ plane}}\ \underbrace{e^{jk_{x_i}x}}_{\substack{unusually\\ phased\\ along\ x}} \tag{58}$$

The modified wave impedance of this unusually phased plane wave (along x) is then the ratio of the E and H field amplitudes

$$\eta_{TE^z_{\phi=90}} = \frac{\eta_i \sin\phi_i}{\sqrt{\cos^2\theta_i \sin^2\phi_i + \sin^2\theta_i}}. \tag{59}$$

Subsequently, using the known formula for the reflection coefficient of a perpendicularly polarized (E-field orthogonal to the yz plane of incidence) plane-wave incident on the planar interface separating two semi-infinite homogeneous media with parameters (η_1, ε_1) and (η_2, ε_2) for the incident and transmit regions, respectively, being [21]

$$\Gamma_\perp = \frac{\eta_2 \cos\theta_i - \eta_1 \cos\theta_t}{\eta_2 \cos\theta_i + \eta_1 \cos\theta_t} \tag{60}$$

where θ_i and θ_t are the angles of the incident and transmitted wave directions measured from the interface normal, the reflection coefficient for the present case of the unusually phased TE^z-polarized plane-wave propagating in the $\phi_i = 90°$ plane may be written as

$$\Gamma_{\perp TE^z_{\phi=90}} = \frac{Z_t \cos\theta_i - \eta_{TE^z_{\phi=90}}}{Z_t \cos\theta_i + \eta_{TE^z_{\phi=90}}} \tag{61}$$

where a zero transmitted angle $\theta_t = 0$ has been assumed upon entering the grooves of the corrugations, and where

$$Z_t = j\frac{g}{d_x}\frac{\omega\mu_g}{k_z}\tan(k_z d) \tag{62}$$

obtained from (37), being the familiar input impedance looking towards a shorted load of a transmission line with length d (modeling the groove) and characteristic impedance taking on the form of a TE wave impedance (since only TE modes assumed inside the grooves due to ACBC; see earlier sections), and with

$$k_z = \sqrt{\omega^2\mu_g\varepsilon_g - k_x^2 - k_y^2} \underset{\substack{inside\\ grooves}}{\overset{k_x=0}{=}} k_0\sqrt{\mu_{rg}\varepsilon_{rg} - \sin^2\theta_i \sin^2\phi_i} \tag{63}$$

where d_x is the period along x of the corrugations, g and d are the width and depth of the grooves, and ($\mu_g = \mu_{rg}\mu_0$, $\varepsilon_g = \varepsilon_{rg}\varepsilon_0$) are the medium parameters of the groove-filling.

Results for the phase, real part and imaginary part of the reflection coefficient produced using (61) for an arbitrary case of corrugations and incidence angles (θ_i, ϕ_i) are given in Fig. 12(a), (b), and (c), respectively. Corresponding results generated by the self-developed full-wave moment-method code [20] are also provided alongside for comparison and as the supreme check. The parameters for this case are: period $d_x = 3.25$ mm, $\varepsilon_{\mathrm{rel,groove}} = 5.42$, depth $d = 9.68$ mm, groove-width $g = 0.716$ mm, $\phi_i = 55.706°$, and $\theta_i = 67.9°$. As seen, the agreement with the full-wave approach is excellent.

B. TM^z Polarized Incidence

Consider next, the TM^z polarized incident plane wave as shown in Fig. 11(b). The fields of this plane wave are stated as

$$\vec{H}^i_{TM^z} = H_0(-\hat{x}\sin\phi_i + \hat{y}\cos\phi_i)e^{j(k_{x_i}x + k_{y_i}y + k_{z_i}z)} \tag{64}$$

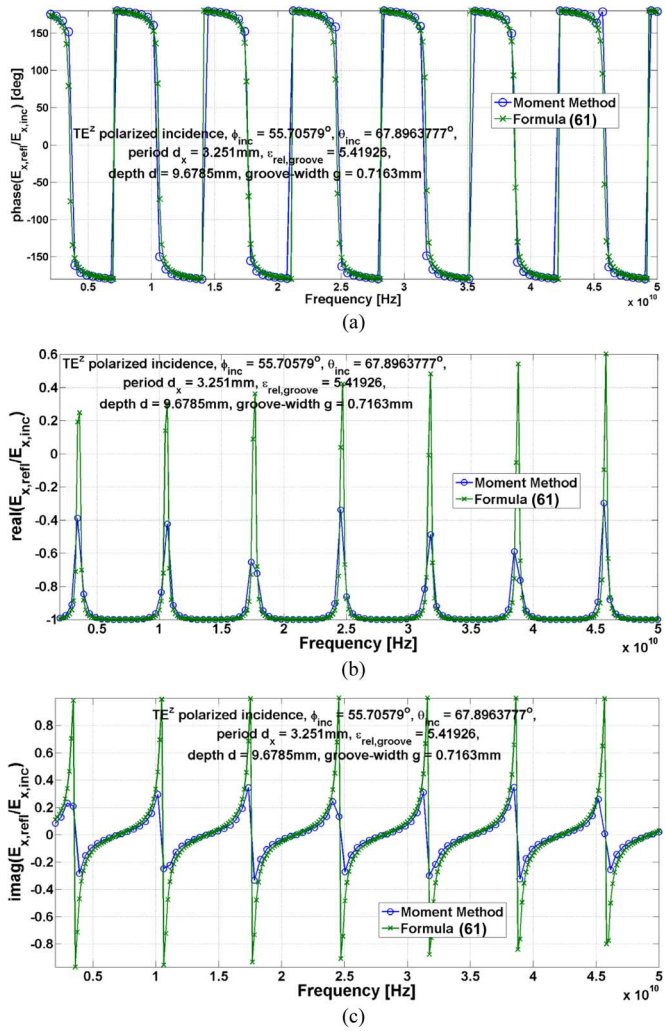

Fig. 12. (a) Phase, (b) real part, and (c) imaginary part of the TE^z reflection coefficient obtained by (61) and compared with moment-method code: for $d_x = 3.251$ mm, $\varepsilon_{\mathrm{rel,groove}} = 5.41926$. depth $d = 9.6785$ mm, groove-width g = 0.7163 mm, $\phi_i = 55.70579°$, and $\theta_i = 67.8963777°$.

$$\begin{aligned}\vec{E}^i_{TM^z} &= \eta_i\left(\vec{H}^i_{TM^z} \times \hat{r}^i\right) \\ &= \eta_i H_0 \begin{pmatrix} -\sin\phi_i \\ \cos\phi_i \\ 0 \end{pmatrix} \\ &\quad \times \begin{pmatrix} -\sin\theta_i\cos\phi_i \\ -\sin\theta_i\sin\phi_i \\ -\cos\theta_i \end{pmatrix} e^{j\left(k_{x_i}x + k_{y_i}y + k_{z_i}z\right)}.\end{aligned} \tag{65}$$

In a similar procedure, extracting only the $\mathrm{TM}_{\phi=0}$ components in the $\Pi = 0\ (xz)$ plane: E_x, E_z and H_y, as shown in (66) and (67) at the bottom of the next page. Again as indicated, these fields are those of a TM^z-polarized plane-wave propagating in the $\phi_i = 0\ (xz)$ plane but with an unusual phase variation along y. The modified wave impedance of this unusually phased plane-wave is

$$\eta_{TM^z_{\phi=0}} = \frac{\eta_i\sqrt{\cos^2\theta_i\cos^2\phi_i + \sin^2\theta_i}}{\cos\phi_i}. \tag{68}$$

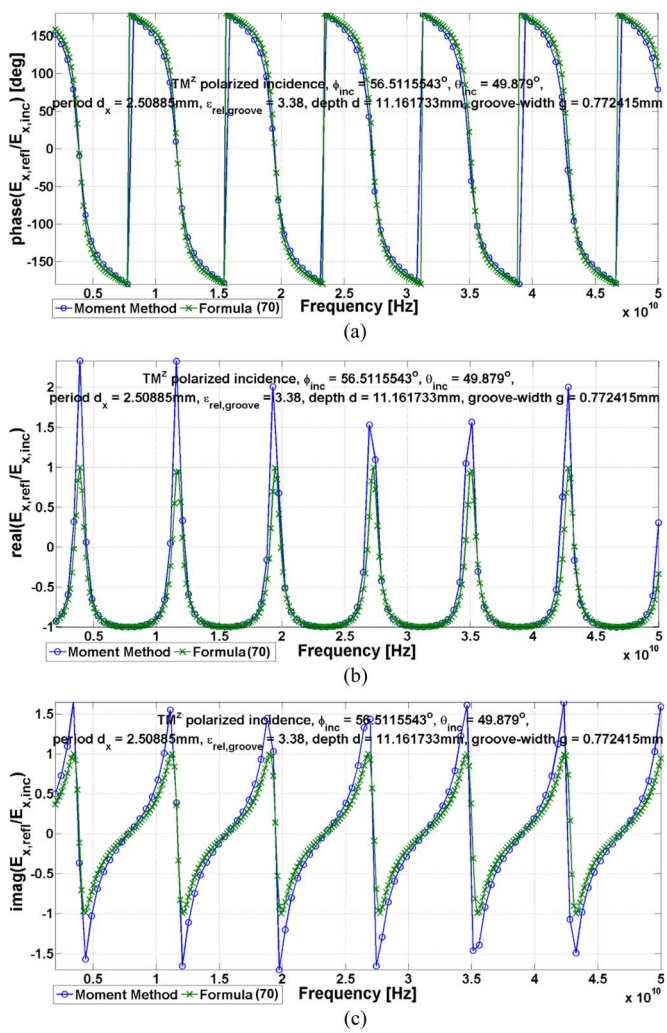

Fig. 13. (a) Phase, (b) real part, and (c) imaginary part of the $\mathbf{TM^z}$ reflection coefficient obtained by (70) and compared with moment-method code: for $d_x = 2.509$ mm, $\varepsilon_{\mathrm{rel,groove}} = 3.38$. depth $d = 11.162$ mm, groove-width g $= 0.7724$ mm, $\phi_i = 56.5115°$, and $\theta_i = 49.879°$.

Using this time the known formula for the reflection coefficient of a parallel-polarized plane-wave incident on the planar interface between two media, being [21]

$$\Gamma_{\parallel} = \frac{\eta_2 \cos\theta_t - \eta_1 \cos\theta_i}{\eta_2 \cos\theta_t + \eta_1 \cos\theta_i} \tag{69}$$

and as before, assuming $\theta_t = 0$ upon penetrating into the grooves, we obtain

$$\Gamma_{\parallel TM^z_{\phi=0}} = \frac{Z_t - \eta_{TM^z_{\phi=0}} \cos\theta_i}{Z_t + \eta_{TM^z_{\phi=0}} \cos\theta_i} \tag{70}$$

where Z_t is the same as that of (62), being still the same TE type wave impedance and *not* the TM type wave impedance as what one might wrongly imagine initially (since TM polarized incident plane wave is presently considered), because no TM^z modes exist inside the grooves under ACBC (see earlier section).

As before, results for the phase, real part and imaginary part of the TM^z reflection coefficient produced using (70) for another arbitrary case of corrugations and incidence angles (θ_i, ϕ_i) are given in Fig. 13(a), (b), and (c), respectively. Corresponding results generated by the self-developed full-wave moment-method code are also provided alongside for comparison and as the supreme check. The parameters for this case are: period $d_x = 2.509$ mm, $\varepsilon_{\mathrm{rel,groove}} = 3.38$, depth $d = 11.162$ mm, groove-width $g = 0.7724$ mm, $\phi_i = 56.5115°$, and $\theta_i = 49.879°$. Evidently, the agreement with the full-wave approach is again seen to be superb.

These direct analytic formulas of (61) and (70) for the TE^z and TM^z complex reflection coefficients (not only the phase or magnitude, but both) of planar corrugations provide speeds of characterization as HIS and AMC surfaces that are higher than most full-wave solvers.

VII. Conclusion

An accurate but yet rapid method for analyzing surface-wave as well as reflection characteristics of planar corrugated surfaces is presented. Based on the use of asymptotic corrugations boundary conditions (ACBC) which yield solutions that approach exactness as the period of the corrugations tends asymptotically to zero, this method is able to treat not only the principal but also oblique azimuth planes of surface-wave propagation (for dispersion analysis) as well as of plane space-wave incidence and reflection (reflection analysis), for both TE and TM polarizations. In addition to the transcendental characteristic equation from which surface-wave dispersion properties (relating frequency to the surface-wavenumber) can be acquired, the formulation of this ACBC-based tool is also capable of producing explicit closed-form analytical expressions for the

$$\vec{E}^{\,i}_{TM^z_{\phi=0}} = \underbrace{\eta_i H_0 \left[\hat{x}(-\cos\theta_i \cos\phi_i) + \hat{z}\sin\theta_i\right] e^{j\left(k_{x_i}x + k_{z_i}z\right)}}_{\text{usual } xz\text{-directed } E\text{-field of TM}^z \text{ polarized plane-wave in } \phi_i=0 \text{ plane}} \underbrace{e^{jk_{y_i}y}}_{\substack{unusually\\ phased\\ along\ y}} \tag{66}$$

$$\vec{H}^{\,i}_{TM^z_{\phi=0}} = \underbrace{\hat{y}(H_0 \cos\phi_i) e^{j\left(k_{x_i}x + k_{z_i}z\right)}}_{\substack{\text{usual } y\text{-directed } H\text{-field of TM}^z \text{ polarized}\\ \text{plane-wave in } \phi_i=0 \text{ plane}}} \underbrace{e^{jk_{y_i}y}}_{\substack{unusually\\ phased\\ along\ y}} \tag{67}$$

fields within both the groove region and the upper half-space above the corrugations, being mathematical functions of all geometrical and material parameters of the corrugated structure. These have potential to serve as facility for the modal analysis of such corrugated surfaces that coexist with other microwave devices, such as mode-matching with waveguides, or even for the analysis of finite corrugations. Furthermore, these field expressions also can find utility in the studies of surface-wave antennas made up of such planar gratings by permitting Fourier integration of the radiating aperture.

Moreover, not only is this ACBC method, for both TE and TM polarizations, better in accuracy than the conventional transverse resonance technique (TRT), the latter already well-reputed for offering quick and accurate insights into the modal dispersion properties, it also provides speedup in computation time as compared to CST Microwave Studio and a moment method code, with reduction in CPU clock times by many thousand-folds, yet without compromising accuracy. This is on top of the fact that the ACBC technique holds up well to full-wave solvers in terms of the ability to provide field expressions, something which the TRT or other asymptotic methods may not offer.

By an unprecedented concept of atypical plane waves that are unusually phased along a transverse direction when propagating within a principal plane, analytical expressions for the complex reflection coefficients of plane-waves impingent on the corrugated surface were also derived for any general oblique azimuth angle of plane-wave incidence, for both TE and TM polarizations. These closed-form mathematical formulas, being functions of all parameters of the corrugation structure as well as the incident plane-wave (its direction and polarization), provide virtually instantaneous acquisition of the complex reflection coefficient, both its real and imaginary parts.

All in all, this proposed new treatment tool for planar corrugations offers improvements over both the classical TRT and the genre of full-wave solvers, in terms of accuracy and the ability to yield field expressions compared with the former, while in terms of speed relative to the latter. It provides fast but yet accurate characterization of EBG structures, HIS/AMC surfaces, soft/hard surfaces, and surface-wave antennas composed of such gratings, in terms of surface-wave dispersion and plane-wave reflection properties, as well as field distributions. This consequently affords likewise swift and effective designs of antennas and microwave devices that make use of such corrugated surfaces.

REFERENCES

[1] H. Goldstein, "Cavity resonators and waveguides containing periodic elements," Ph.D. dissertation, Mass. Inst. of Technol., Cambridge, MA, USA, 1943.

[2] H. Goldstein, "The theory of corrugated transmission lines and waveguides," MIT Radiation Lab, Rep. 494, Arp. 1944, pp. 1–17.

[3] G. Goubau, "Surface waves and their application to transmission lines," *J. Appl. Phys.*, vol. 21, pp. 1119–1128, Nov. 1950.

[4] A. Sommerfeld*, Ann. d. Physik*, vol. 28, p. 665, 1909.

[5] R. S. Elliott, "On the theory of corrugated plane surfaces," *IRE Trans. Antennas Propag.*, pp. 71–81, Apr. 1954.

[6] G. Piefke, "The transmission characteristics of a corrugated guide," *IRE Trans. Antennas Propag.*, pp. 183–190, Dec. 1959.

[7] R. W. Hougardy and R. C. Hansen, "Scanning surface wave antennas—Oblique surface waves over a corrugated conductor," *IRE Trans. Antennas Propag.*, pp. 370–376, Oct. 1958.

[8] H. A. Kalhor, "Numerical evaluation of Rayleigh hypothesis for analyzing scattering from corrugated gratings—TE polarization," *IEEE Trans. Antennas Propag.*, vol. AP-24, no. 6, pp. 884–889, Nov. 1976.

[9] J. P. Kim, C. W. Lee, and H. Son, "Analysis of corrugated surface wave antenna using hybrid MOM/UTD technique," *IEE Elect. Lett.*, vol. 35, no. 5, pp. 353–354, Mar. 1999.

[10] E. Alfonso, A. Valero-Nogueira, J. I. Herranz, and F. Vico, "Moment method analysis of corrugated surfaces using the aperture integral equation," *IEEE Trans. Antennas Propag.*, vol. 57, no. 7, pp. 2208–2212, Jul. 2009.

[11] P.-S. Kildal, "Artificially soft and hard surfaces in electromagnetics," *IEEE Trans. Antennas Propag.*, vol. 38, no. 10, pp. 1537–1544, Oct. 1990.

[12] P.-S. Kildal, A. A. Kishk, and A. Tengs, "Reduction of forward scattering from cylindrical objects using hard surfaces," *IEEE Trans. Antennas Propag.*, vol. 44, no. 11, pp. 1509–1520, Nov. 1996.

[13] Z. Ying and P.-S. Kildal, "Improvements of dipole, helix, spiral, microstrip patch and aperture antennas with ground planes by using corrugated soft surfaces," *IEE Proc. Microw., Antennas, Propag.*, vol. 143, no. 3, pp. 244–248, Jun. 1996.

[14] T. B. A. Senior and J. L. Volakis, "Generalized impedance boundary conditions in scattering," *Proc. IEEE*, vol. 79, no. 10, pp. 1413–1420, Oct. 1991.

[15] T. B. A. Senior and J. L. Volakis*, Approximate Boundary Conditions in Electromagnetics*. Stevenage, U.K.: IET, "," *IET IEEE Electromagnetic Waves Series*, 1995.

[16] H. A. Kalhor, "Approximate analysis of electromagnetic scattering from corrugating conducting surfaces by surface impedance modeling," *IEEE Trans. Antennas Propag.*, vol. AP-25, pp. 721–722, Sep. 1977.

[17] I. Hanninen and K. Nikoskinen, "Implementation of method of moments for numerical analysis of corrugated surfaces with impedance boundary condition," *IEEE Trans. Antennas Propag.*, vol. 56, no. 1, pp. 278–281, Jan. 2008.

[18] T. M. Uusitupa, "Usability studies on approximate corrugation models in scattering analysis," *IEEE Trans. Antennas Propag.*, vol. 54, no. 9, pp. 2486–2496, Sep. 2006.

[19] P.-S. Kildal, A. Kishk, and Z. Sipus, "Asymptotic boundary conditions for strip-loaded and corrugated surfaces," *Microw. Opt. Technol. Lett.*, vol. 14, no. 2, pp. 99–101, Feb. 1997.

[20] M. Ng Mou Kehn, "Moment method analysis of plane-wave scattering from planar corrugated surfaces using parallel-plate cavity Green's functions and derivation of analytic reflection-phase formulas for both polarizations and oblique azimuth planes," *Radio Sci.*, vol. 47, p. RS3008, Jun. 2012, 10.1029/2011RS004938.

[21] C. A. Balanis*, Advanced Engineering Electromagnetics*. New York, NY, USA: Wiley.

Malcolm Ng Mou Kehn (S'02–M'06) was born in Singapore on September 26, 1976. He received the B.Eng. (honors) degree from the National University of Singapore, Singapore, in 2001, and the Licentiate and Ph.D. degrees from Chalmers University of Technology, Gothenburg, Sweden, in 2004 and 2005, respectively, all in electrical engineering.

During 2006–2008, he was a Postdoctoral Fellow in the Department of Electrical and Computer Engineering, University of Manitoba, Winnipeg, MB, Canada. Following this, he proceeded to Concordia University, Montreal, QC, Canada, for a year. In August 2009, he joined the Department of Electrical Engineering, National Chiao Tung University, Hsinchu, Taiwan, first as an Assistant Professor and then as an Associate Professor since August 2012. He had been actively involved in research projects funded by the Swedish Defense Research Agency between 2002 and 2006. During autumn 2004, he spent several months at the University of Siena, Italy, for a research visit. In December 2004, he visited the University of Zagreb, Croatia, as an invited speaker where he gave an IEEE lecture, in connection with the IEEE Croatia Chapter activities. Throughout 2006 to 2009, he worked extensively on numerous projects supported by Canadian industry and national research bodies. Since August 2009, he has been securing research project grants funded by the National Science Council of Taiwan.

Dr. Ng Mou Kehn received the Union Radio-Scientifique Internationale (URSI) Young Scientist Award in 2007.